JOURNAL OF SPACECRAFT AND ROCKETS
Vol. 34, No. 4, July–August 1997

Improved Matched Asymptotic Solutions for Three-Dimensional Atmospheric Skip Trajectories

Zeal-Sain Kuo*
Chung Cheng Institute of Technology, Tao-Yuan, Taiwan 33509, Republic of China
and
Nguyen X. Vinh†
University of Michigan, Ann Arbor, Michigan 48109-2118

An improved technique for matching the asymptotic solutions of nonlinear differential equations is presented and successfully applied to the three-dimensional atmospheric skip trajectories. The classic method of matched asymptotic expansions is generally applied to two-boundary value problems. When we apply the classic method to initial value problems, because of error propagation, the resulting accuracy usually depends on physical problems. In the proposed technique, second-order solutions are obtained by first generating a set of equations for the small perturbations, which are the discrepancies between the uniformly valid first-order solutions and the exact solutions. Then, the equations of the small perturbations are integrated separately near the outer and inner boundaries to obtain the perturbed outer and inner expansion solutions, respectively, for second-order matching. In addition, in this improved technique the endpoint boundaries are artificially extended or constructed to strengthen the physical assumptions on the outer and inner expansions for matching. Compared with the solutions obtained by numerical integration over a wide range of entry conditions, the second-order solutions obtained by this improved technique are very accurate. The trajectory elements at the lowest altitude and at exit, as well as their accuracy, are evaluated.

Nomenclature

A = aerodynamic reference area, m^2
B = lumped parameter defined by Eq. (8)
C_D = drag coefficient
C_D^* = drag coefficient at maximum lift-to-drag ratio
C_L = lift coefficient
C_L^* = lift coefficient at maximum lift-to-drag ratio
E = lift-to-drag ratio
E^* = maximum lift-to-drag ratio
g = gravitational acceleration, m/s^2
h = dimensionless altitude variable
m = vehicle mass, kg
r = radius altitude, m
t = time, s
u = dimensionless speed variable
V = velocity, m/s
β = inverse atmospheric scale height, m^{-1}
γ = flight-path angle, deg
θ = down-range angle or longitude, deg
λ = normalized lift coefficient
ρ = density, kg/m^3
σ = bank angle, deg
ϕ = cross-range angle or latitude, deg
ψ = heading angle, deg

Subscripts

b = variables at bottom
i = variables at initial state
mc = modified composite solutions
s = reference sea level

Superscripts

c = composite solutions
i = inner expansions
o = outer expansions

Introduction

WITH the advent of manned space explorations and the establishment of permanent space stations, the safe recovery of an orbiting aerospace vehicle, or its orbital maneuver with minimum fuel consumption, has been one of the most challenging technologies in space flight dynamics. During atmospheric passage, there is a tremendous change in speed, kinetic energy, dynamic pressure, and heating rate. It is then of interest to have explicit analytical solutions for variations of the elements of the three-dimensional entry trajectory because the heading change due to three-dimensional motion has promising applications in aeroassisted orbital transfer. A powerful method for analyzing dynamic systems governed by equations with the dominant forces varying widely between the two endpoints is the method of matched asymptotic expansions (MAE). This technique, initiated by aerodynamicists,[1,2] has been successfully applied to problems in astrodynamics.[3,4] By using this method, some analytical solutions for atmospheric re-entry problems have been obtained, but they are restricted to first-order solutions.[5–7] In this paper, we propose an improved technique[8] to go beyond the first-order solutions reported previously. In this improved technique, the perturbation equations are generated by considering the small discrepancies between the exact solutions and the uniformly valid first-order solutions. Then, the equations for the small perturbations are integrated separately near the outer and inner boundaries to obtain the perturbed outer and inner expansion solutions, respectively, for second-order matching.

To illustrate the applicability of the improved MAE (iMAE), the proposed technique is applied to analyze the three-dimensional atmospheric re-entry problem. We obtain, in addition to the usual solutions for the altitude, speed, and flight-path-angle variables, second-order solutions for the heading, latitude, and longitude in explicit form with excellent accuracy. The explicit second-order solutions are compared with the pure numerical solutions, and the errors incurred are assessed to show the region of validity for application of the technique.

Presented as Paper 96-3596 at the AIAA/AAS Astrodynamics Specialist Conference, San Diego, CA, July 29–31, 1996; received Nov. 18, 1996; revision received April 10, 1997; accepted for publication April 10, 1997.

*Associate Professor, Department of Mechanical Engineering. Member AIAA.
†Professor, Department of Aerospace Engineering. Member AIAA.

Equations of Motion

Consider the three-dimensional flight trajectory of a space vehicle entering a nonrotating planetary atmosphere. Using the standard notation as shown in Fig. 1, we have the governing equations

$$\frac{dr}{dt} = V\sin\gamma \qquad \frac{dV}{dt} = -\frac{\rho A C_D V^2}{2m} - g\sin\gamma$$
$$V\frac{d\gamma}{dt} = \frac{\rho A C_L V^2}{2m}\cos\sigma - \left(g - \frac{V^2}{r}\right)\cos\gamma \tag{1}$$
$$V\frac{d\psi}{dt} = \frac{\rho A C_L V^2}{2m\cos\gamma}\sin\sigma - \frac{V^2}{r}\cos\gamma\cos\psi\tan\phi$$
$$\frac{d\phi}{dt} = \frac{V\cos\gamma\sin\psi}{r} \qquad \frac{d\theta}{dt} = \frac{V\cos\gamma\cos\psi}{r\cos\phi}$$

For a Newtonian inverse-square gravitational field, we have

$$g/g_s = r_s^2/r^2 \tag{2}$$

We define the dimensionless variables

$$u = V^2/g_s r_s \qquad h = (r - r_s)/r_s \tag{3}$$

Furthermore, we use a strictly exponential atmosphere of the form

$$\rho = \rho_s e^{-h/\varepsilon} \qquad \varepsilon = 1/\beta r_s \tag{4}$$

where ε is a small dimensionless parameter.

The lift and drag coefficients are assumed to be of the form

$$C_L = \lambda C_L^* \tag{5}$$

and

$$C_D = C_D^*(1 + \lambda^2)/2 \tag{6}$$

Then, by using the dimensionless altitude h as the independent variable to replace the time variable, we have the dimensionless equations of motion

$$\frac{du}{dh} = -\frac{2}{(1+h)^2} - \frac{B(1+\lambda^2)ue^{-h/\varepsilon}}{\varepsilon E^*\sin\gamma}$$
$$\frac{d\gamma}{dh} = \left[\frac{1}{(1+h)} - \frac{1}{u(1+h)^2}\right]\frac{1}{\tan\gamma} + \frac{B\lambda\cos\sigma e^{-h/\varepsilon}}{\varepsilon\sin\gamma} \tag{7}$$
$$\frac{d\psi}{dh} = -\frac{\cos\psi\tan\phi}{(1+h)\tan\gamma} + \frac{B\lambda\sin\sigma e^{-h/\varepsilon}}{\varepsilon\sin\gamma\cos\gamma}$$
$$\frac{d\phi}{dh} = \frac{\sin\psi}{(1+h)\tan\gamma} \qquad \frac{d\theta}{dh} = \frac{\cos\psi}{(1+h)\tan\gamma\cos\phi}$$

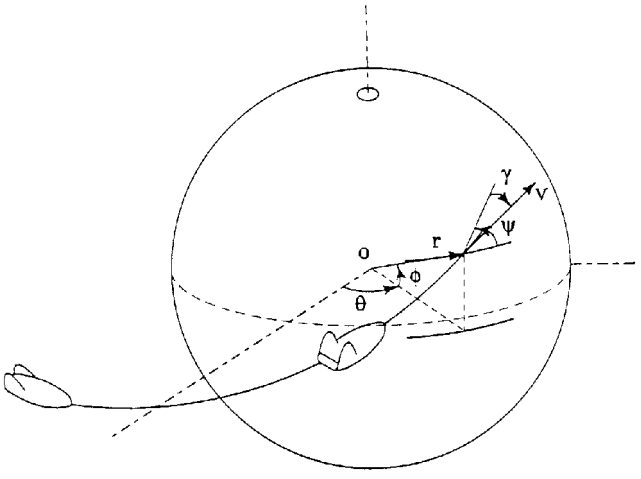

Fig. 1 Coordinate system with trajectory variables.

In these equations, the small dimensionless parameter ε represents the planetary atmosphere characteristic. For the Earth's atmosphere, the practical value of $\varepsilon = \frac{1}{900}$. Furthermore, the maximum lift-to-drag ratio $E^* = C_L^*/C_D^*$ represents the performance characteristic of the lifting vehicle; other physical parameters are lumped together in the coefficient B defined as

$$B = \frac{\rho_s A C_L^*}{2m\beta} \tag{8}$$

The flight program is specified by the normalized lift coefficient λ and the bank angle σ.

The system equation (7) constitutes the most appropriate dimensionless system of equations for analyzing entry into a planetary atmosphere with lift and bank modulation. To generate the three-dimensional entry trajectory, it suffices to select a lift control $\lambda(h)$ and a bank angle $\sigma(h)$ as functions of the altitude and integrate the equations from the initial condition $[u_i, \gamma_i, \psi_i, \phi_i, \theta_i]$ at entry altitude h_i. In subsequent computation, we use a constant angle of attack, that is, a constant λ and a constant bank angle σ for the flight.

Integration by MAE

By using the matched asymptotic expansions method, we obtain separately the outer solutions at high altitude by retaining in the equations only the dominant gravitational and centrifugal force and the inner solutions at low altitude by keeping only the strong aerodynamic force. By using appropriate matching, a composite solution uniformly valid over the whole entry trajectory is then obtained.

Outer Expansions (Keplerian Region)

The outer expansions describe the behavior of motion in the region near the vacuum. At high altitude in the limiting case, $e^{-h/\varepsilon} \to 0$, the aerodynamic force nearly disappears when compared with the combination of gravitational and centrifugal forces. Therefore, we obtain the outer expansions by repeated application of the outer limit, $\varepsilon \to 0$, with the altitude variable h and other variables held fixed. We consider the state vector $\boldsymbol{x} = [u, \gamma, \psi, \phi, \theta]$ and assume the following expansions:

$$\boldsymbol{x}^o = \boldsymbol{x}_0(h) + \varepsilon\boldsymbol{x}_1(h) + \varepsilon^2\boldsymbol{x}_2(h) + \cdots \tag{9}$$

By substituting into the system equation (7) and taking the outer limit, the first-order equations for the outer expansions are

$$\frac{du_0}{dh} = -\frac{2}{(1+h)^2} \qquad \frac{d\gamma_0}{dh} = \left\{\frac{1}{(1+h)} - \frac{1}{u_0(1+h)^2}\right\}\frac{1}{\tan\gamma_0}$$
$$\frac{d\psi_0}{dh} = -\frac{\cos\psi_0\tan\phi_0}{(1+h)\tan\gamma_0} \qquad \frac{d\phi_0}{dh} = \frac{\sin\psi_0}{(1+h)\tan\gamma_0} \tag{10}$$
$$\frac{d\theta_0}{dh} = \frac{\cos\psi_0}{(1+h)\tan\gamma_0\cos\phi_0}$$

These are the equations for three-dimensional Keplerian motion in the vacuum. Upon integrating, the outer solutions are

$$u_0 = \frac{2}{(1+h)} + C_1 \qquad \cos\gamma_0 = \frac{C_2}{\sqrt{C_1(1+h)^2 + 2(1+h)}}$$
$$\cos\psi_0 = \frac{C_3}{\cos\phi_0} \tag{11}$$
$$\sin\phi_0 = \sqrt{1 - C_3^2}\sin\left(\cos^{-1}\left\{\frac{1 - \left[C_2^2/(1+h)\right]}{\sqrt{1 + C_1C_2^2}}\right\} + C_4\right)$$
$$\cos(\theta_0 - C_5) = \cos\left(\cos^{-1}\left\{\frac{1 - \left[C_2^2/(1+h)\right]}{\sqrt{1 + C_1C_2^2}}\right\} + C_4\right)\Big/\cos\phi_0$$

where $C_n, n = 1, 2, \ldots, 5$ are the constants of integration to be determined after matching.

Inner Expansions (Aerodynamic Predominant Region)

Near the surface of the planet, the aerodynamic force is dominant. The inner expansions are obtained by repeated application of the inner limit, which is defined as the limit when $\varepsilon \to 0$ with the new altitude variable $\bar{h} = h/\varepsilon$ and the other dimensionless variables held fixed. We assume the following expansion:

$$\boldsymbol{x}^i = \bar{\boldsymbol{x}}_0(\bar{h}) + \varepsilon\bar{\boldsymbol{x}}_1(\bar{h}) + \varepsilon^2\bar{\boldsymbol{x}}_2(\bar{h}) + \cdots \tag{12}$$

By substituting into the system equation (7) and taking the inner limit, the first-order equations for the inner expansions are

$$\frac{\mathrm{d}\bar{u}_0}{\mathrm{d}\bar{h}} = -\frac{B(1+\lambda^2)\bar{u}_0 e^{-\bar{h}}}{E^* \sin\bar{\gamma}_0} \qquad \frac{\mathrm{d}\bar{\gamma}_0}{\mathrm{d}\bar{h}} = \frac{B\lambda\cos\sigma e^{-\bar{h}}}{\sin\bar{\gamma}_0}$$
$$\frac{\mathrm{d}\bar{\psi}_0}{\mathrm{d}\bar{h}} = \frac{B\lambda\sin\sigma e^{-\bar{h}}}{\sin\bar{\gamma}_0\cos\bar{\gamma}_0} \qquad \frac{\mathrm{d}\bar{\phi}_0}{\mathrm{d}\bar{h}} = 0 \qquad \frac{\mathrm{d}\bar{\theta}_0}{\mathrm{d}\bar{h}} = 0 \tag{13}$$

This system can also be integrated to yield the inner solutions

$$\bar{u}_0 = \bar{C}_1 \exp\left[-\frac{(1+\lambda^2)}{\lambda E^*\cos\sigma}\bar{\gamma}_0\right] \qquad \cos\bar{\gamma}_0 = B\lambda\cos\sigma e^{-\bar{h}/\varepsilon} + \bar{C}_2$$
$$\bar{\psi}_0 = \tan\sigma\,\ell n(\sec\bar{\gamma}_0 + \tan\bar{\gamma}_0) + \bar{C}_3 \qquad \bar{\phi}_0 = \bar{C}_4 \qquad \bar{\theta}_0 = \bar{C}_5 \tag{14}$$

where $\bar{C}_n, n = 1, 2, \ldots, 5$ are the corresponding constants of integration.

First-Order Composite Solutions

To have the solutions uniformly valid over both the outer and the inner regions, we construct the composite solutions by taking the sum of the outer and inner solutions and subtracting the parts they have in common:

$$\boldsymbol{x}_c = \boldsymbol{x}_0 + \bar{\boldsymbol{x}}_0 - \boldsymbol{x}_{00} \tag{15}$$

where $\boldsymbol{x}_{00}$ is the common limit. To avoid state variables becoming imaginary before the vehicle reaches the lowest altitude, we require that at a certain altitude, h_b, the composite solution γ_c and the inner solution $\bar{\gamma}_0$ reach zero simultaneously, that is,

$$\bar{\gamma}_0(h_b/\varepsilon) = \gamma_c(h = h_b) = 0 \tag{16}$$

Hence, for matching, we choose a modified common limit so that Eq. (16) is satisfied:

$$\boldsymbol{x}_{00} = \lim_{h\to h_b}\boldsymbol{x}_0(h) = \lim_{\bar{h}\to\infty}\bar{\boldsymbol{x}}_0(\bar{h}) \tag{17}$$

i.e.,

$$u_{00} = \frac{2}{1+h_b} + C_1 = \bar{C}_1\exp\left[-\frac{(1+\lambda^2)}{\lambda E^*\cos\sigma}\gamma_{00}\right]$$
$$\cos\gamma_{00} = \frac{C_2}{\sqrt{C_1(1+h_b)^2 + 2(1+h_b)}} = \bar{C}_2$$
$$\psi_{00} = \cos^{-1}\left(\frac{C_3}{\cos\phi_{00}}\right) = \tan\sigma\,\ell n[\sec\gamma_{00} + \tan\gamma_{00}] + \bar{C}_3 \tag{18}$$
$$\sin\phi_{00} = \sqrt{1-C_3^2}\sin\left(\cos^{-1}\left\{\frac{1-\left[C_2^2/(1+h_b)\right]}{\sqrt{1+C_1C_2^2}}\right\} + C_4\right) = \sin\bar{C}_4$$
$$\cos(\theta_{00} - C_5) = \cos\left(\cos^{-1}\left\{\frac{1-\left[C_2^2/(1+h_b)\right]}{\sqrt{1+C_1C_2^2}}\right\} + C_4\right)\Big/\cos\phi_{00} = \cos(\bar{C}_5 - C_5)$$

Then, according to Eq. (15), the first-order composite solutions are

$$u_c = \frac{2}{1+h} + \bar{C}_1\exp\left[-\frac{(1+\lambda^2)}{\lambda E^*\cos\sigma} \times \cos^{-1}\left(B\lambda\cos\sigma e^{-h/\varepsilon} + \bar{C}_2\right)\right] - \frac{2}{1+h_b}$$
$$\cos\gamma_c = \frac{C_2}{\sqrt{C_1(1+h)^2 + 2(1+h)}} + B\lambda\cos\sigma e^{-h/\varepsilon} - \frac{C_2}{\sqrt{C_1(1+h_b)^2 + 2(1+h_b)}}$$
$$\psi_c = \cos^{-1}\left(\frac{C_3}{\cos\phi_c}\right) + \tan\sigma\,\ell n(\sec\bar{\gamma}_0 + \tan\bar{\gamma}_0) + \bar{C}_3 - \cos^{-1}\left(\frac{C_3}{\cos\phi_{00}}\right) \tag{19}$$
$$\sin\phi_c = \sqrt{1-C_3^2}\sin\left(\cos^{-1}\left\{\frac{1-\left[C_2^2/(1+h)\right]}{\sqrt{1+C_1C_2^2}}\right\} + C_4\right)$$
$$\cos(\theta_c - C_5) = \cos\left(\cos^{-1}\left\{\frac{1-\left[C_2^2/(1+h)\right]}{\sqrt{1+C_1C_2^2}}\right\} + C_4\right)\Big/\cos\phi_c$$

From the second of Eqs. (19), at the lowest altitude we have

$$1 = B\lambda\cos\sigma e^{-h_b/\varepsilon} + \bar{C}_2 \tag{20}$$

Now, there are 11 unknowns, namely, the 10 constants of integration and the lowest altitude h_b. If we set the initial conditions $[u_i, \gamma_i, \psi_i, \phi_i, \theta_i]$ at h_i in the composite solution equations (19) to be identically satisfied, these five new equations, together with Eqs. (18) and (20), constitute a system of 11 equations for 11 unknowns. Because the first two variables, u and γ, are independent of the other variables, ψ, ϕ, and θ, we can first solve for C_1, C_2, $\bar{C}_1$, $\bar{C}_2$, and h_b. Next, from the relevant equations, we solve for C_3, C_4, $\bar{C}_3$, and $\bar{C}_4$. Finally, the constants of integration C_5 and $\bar{C}_5$ for θ can be evaluated by satisfying the matching condition and the initial condition for θ at h_i. With the constants evaluated, Eqs. (19) are the first-order composite solutions in terms of the altitude variable h.

Second-Order Solutions

We construct the second-order solutions by considering the small discrepancies between the first-order composite solutions and the exact solutions. Let

$$u = u_c + z = u_0 + \bar{u}_0 - u_{00} + z$$
$$\cos\gamma = \cos\gamma_c + q = \cos\gamma_0 + \cos\bar{\gamma}_0 - \cos\gamma_{00} + q$$
$$\psi = \psi_c + y = \psi_0 + \bar{\psi}_0 - \psi_{00} + y \tag{21}$$
$$\phi = \phi_c + f = \phi_0 + \bar{\phi}_0 - \phi_{00} + f = \phi_0 + f$$
$$\theta = \theta_c + p = \theta_0 + \bar{\theta}_0 - \theta_{00} + p = \theta_0 + p$$

Note that, because the inner solutions $\bar{\phi}_0$ and $\bar{\theta}_0$ are constants, they are canceled by their common limits ϕ_{00} and θ_{00}, respectively. As a consequence, the classic first-order composite solutions for θ and ϕ are not sufficiently accurate because they are simply the Keplerian solutions. By substituting Eq. (21) into the dimensionless equations for motion, Eqs. (7), and using the equations of outer and inner expansions for simplification, we obtain the equations for the small perturbations

$$\frac{\mathrm{d}z}{\mathrm{d}h} = -\frac{B(1+\lambda^2)ue^{-h/\varepsilon}}{\varepsilon E^*\sin\gamma} + \frac{B(1+\lambda^2)\bar{u}_0 e^{-h/\varepsilon}}{\varepsilon E^*\sin\bar{\gamma}_0}$$
$$\frac{\mathrm{d}q}{\mathrm{d}h} = -\left\{\frac{1}{(1+h)} - \frac{1}{u(1+h)^2}\right\}\cos\gamma + \left\{\frac{1}{(1+h)} - \frac{1}{u_0(1+h)^2}\right\}\cos\gamma_0$$

$$\frac{dy}{dh} = -\frac{1}{(1+h)}\left(\frac{\cos\psi\tan\phi}{\tan\gamma} - \frac{\cos\psi_0\tan\phi_0}{\tan\gamma_0}\right)$$
$$+\left(\frac{B\lambda\sin\sigma e^{-h/\varepsilon}}{\varepsilon\sin\gamma\cos\gamma} - \frac{B\lambda\sin\sigma e^{-h/\varepsilon}}{\varepsilon\sin\bar{\gamma}_0\cos\bar{\gamma}_0}\right)$$
$$\frac{df}{dh} = \frac{1}{(1+h)}\left(\frac{\sin\psi}{\tan\gamma} - \frac{\sin\psi_0}{\tan\gamma_0}\right)$$
$$\frac{dp}{dh} = \frac{1}{(1+h)}\left(\frac{\cos\psi}{\tan\gamma\cos\phi} - \frac{\cos\psi_0}{\tan\gamma_0\cos\phi_0}\right) \tag{22}$$

The initial conditions for the perturbations are trivially

$$z(h_i) = 0 \qquad q(h_i) = 0 \qquad y(h_i) = 0$$
$$f(h_i) = 0 \qquad p(h_i) = 0 \tag{23}$$

We integrate the equations for the perturbations separately, first in the outer region and then in the inner region.

Second-Order Solutions for u and γ

Because the equations for u and γ are decoupled from the system, we can integrate the first two equations by assuming the outer expansions for the perturbations:

$$z^o = z_0(h) + \varepsilon z_1(h) + \varepsilon^2 z_2(h) + \cdots$$
$$q^o = q_0(h) + \varepsilon q_1(h) + \varepsilon^2 q_2(h) + \cdots \tag{24}$$

By taking the outer limit, $\varepsilon \to 0$, and keeping other variables fixed, we obtain the outer solutions for the perturbation z:

$$\frac{dz_0}{dh} = 0 \Rightarrow z_0 = C_6 \tag{25}$$

It can be shown that C_6 is zero. Then, upon using this solution and integrating, the outer solution for perturbation q is

$$q_0 = \frac{C_7}{\sqrt{C_1(1+h)^2 + 2(1+h)}} \tag{26}$$

where C_7 is the constant of integration.

For the inner solution z, because $\sin\gamma$ tends to $\sin\bar{\gamma}_0$ and is very small, by inspecting the first of the perturbation equations, we find that u is very close to $\bar{u}_0$. This makes the evaluation of z very sensitive to errors. Because the first-order composite solution for u is sufficiently accurate, we concentrate on improving the solution for perturbation of the flight-path angle in the inner region. First, we anticipate the inner expansions for the perturbations in the form

$$z^i = \bar{z}_0(\bar{h}) + \varepsilon\bar{z}_1(\bar{h}) + \varepsilon^2\bar{z}_2(\bar{h}) + \cdots$$
$$q^i = \varepsilon\left[\bar{q}_0(\bar{h}) + \varepsilon\bar{q}_1(\bar{h}) + \varepsilon^2\bar{q}_2(\bar{h}) + \cdots\right] \tag{27}$$

Next, we use the following limiting and approximate conditions:

$$u \to \bar{u}_0 + z \approx \bar{u}_0 \qquad z \ll 1$$
$$\cos\gamma \to \cos\bar{\gamma}_0 + q \approx \cos\bar{\gamma}_0 \qquad q \ll 1 \tag{28}$$
$$1 + h \to 1 + h_b$$

By taking the inner limit and keeping other variables fixed, we obtain the equation for $\bar{q}_0$:

$$\frac{d\bar{q}_0}{d\bar{h}} = -\left\{\frac{1}{(1+\varepsilon\bar{h})} - \frac{1}{\bar{u}_0(1+h_b)^2}\right\}\cos\bar{\gamma}_0$$
$$+\left\{\frac{1}{(1+\varepsilon\bar{h})} - \frac{1}{u_0(1+\varepsilon\bar{h})^2}\right\}\cos\gamma_0 \tag{29}$$

Note that in Eq. (29) we keep the integrable terms in an exact form to increase accuracy and make the form of the final solution simple. Therefore, it is only in the second term that $\varepsilon\bar{h}$ is replaced by h_b.

Upon integrating, we have the inner solution for perturbation q in the form

$$\bar{q}_0 = f(\bar{h}) + \bar{C}_7 \tag{30}$$

The expression for $f(\bar{h})$ is very complex so we discuss only its application here. We use this solution, Eq. (30), and the outer solution q_0 in Eq. (26) to construct the composite solution $q_c(h)$, satisfying identically the initial condition $q(h_i) = 0$. Then, the second-order solution for γ is

$$\cos\gamma^c = \cos\gamma_c + q_c$$
$$= \frac{C_2}{\sqrt{C_1(1+h)^2 + 2(1+h)}} + B\lambda\cos\sigma e^{-h/\varepsilon} + q_c(h) \tag{31}$$

As compared to the first-order composite solution given by the second expression of Eqs. (19), besides the additional second-order term $q(h)$, we reevaluate all of the constants of integration to construct a modified second-order solution in the form

$$\cos\gamma_m^c = \cos\gamma_{\rm mc} + q_{\rm mc}$$
$$= \frac{C_2'}{\sqrt{C_1'(1+h)^2 + 2(1+h)}} + B\lambda\cos\sigma e^{-h/\varepsilon} + q_{\rm mc}(h) \tag{32}$$

such that

$$B\lambda\cos\sigma e^{-h_b'/\varepsilon} + \bar{C}_2' + q_{\rm mc}(h_b') = 1 \tag{33}$$

where $\cos\gamma_{\rm mc}$ is the modified first-order composite solution and $q_{\rm mc}$ is the composite solution for q but now denoting the difference between the $\cos\gamma_{\rm mc}$ and the exact solution. The solution for u is the modified first-order solution with new values for the constants and the bottom altitude:

$$u_{\rm mc} = \frac{2}{1+h} + \bar{C}_1'\exp\left[-\frac{(1+\lambda^2)}{\lambda E^*\cos\sigma}\right.$$
$$\left.\times\cos^{-1}\left(B\lambda\cos\sigma e^{-h/\varepsilon} + \bar{C}_2'\right)\right] - \frac{2}{1+h_b'} \tag{34}$$

Equations (32) and (34) are now the improved composite solutions for u and γ in three-dimensional skip trajectory. The constants of integration C_1', C_2', $\bar{C}_1'$, $\bar{C}_2'$ and the lowest altitude h_b' are evaluated from Eq. (33), together with the first two expressions of Eq. (19), with the accented constants and Eqs. (32) and (34) satisfying the initial conditions $u_{\rm mc} = u_i$ and $\gamma_m^c = \gamma_i$ at the initial altitude $h = h_i$.

For the second-order solution of ψ, by inspecting the third equation of the perturbation equations (22), we observe that the equation for perturbation y has the same difficulty in sensitivity that we encountered in solving perturbation z. We then concentrate on solving the second-order solutions for ϕ and θ.

Second-Order Solutions for ϕ and θ

The second-order solutions for ϕ and θ are obtained by integrating the perturbation equations for f and p in Eq. (22). The solutions in the outer region are trivially zero. For the inner region, by changing the independent variable to $\bar{\gamma}_0$ for the integration, we obtain

$$\bar{f}_0 = \left\{\tan\sigma[F_1(\bar{\gamma}_0) + \bar{C}_2F_2(\bar{\gamma}_0)] + \bar{C}_3[\bar{\gamma}_0 + \bar{C}_2F_3(\gamma_0)] + \cdots\right.$$
$$\left.+\frac{\sin\psi_{00}}{\tan\gamma_{00}}\ell_n(\cos\bar{\gamma}_0 - \bar{C}_2)\right\}\frac{1}{(1+h_b)} + \bar{C}_9$$
$$\bar{p}_0 = \left(\bar{\gamma}_0 + \bar{C}_2F_3(\bar{\gamma}_0) + \frac{\cos^2\psi_{00}}{C_3\tan\gamma_{00}}\ell_n(\cos\bar{\gamma}_0 - \bar{C}_2)\right.$$
$$\left.-\frac{1}{2!}\{2\bar{C}_3\tan\sigma[F_1(\bar{\gamma}_0) + \bar{C}_2F_2(\bar{\gamma}_0)]\} + \cdots\right)\frac{1}{(1+h_b)} + \bar{C}_{10} \tag{35}$$

where $\bar{C}_9$ and $\bar{C}_{10}$ are the corresponding constants of integration. Note that the prime for $\bar{C}_2$ and h_b, which represents the new constants

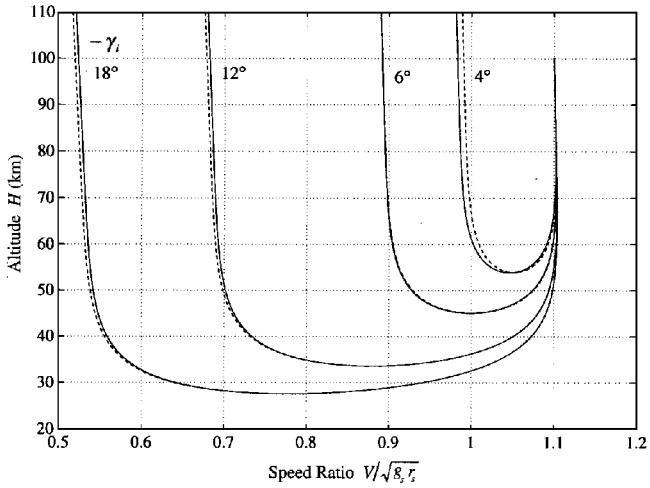

Fig. 2 Variation of speed as a function of altitude for various entry angles in three-dimensional skip trajectory.

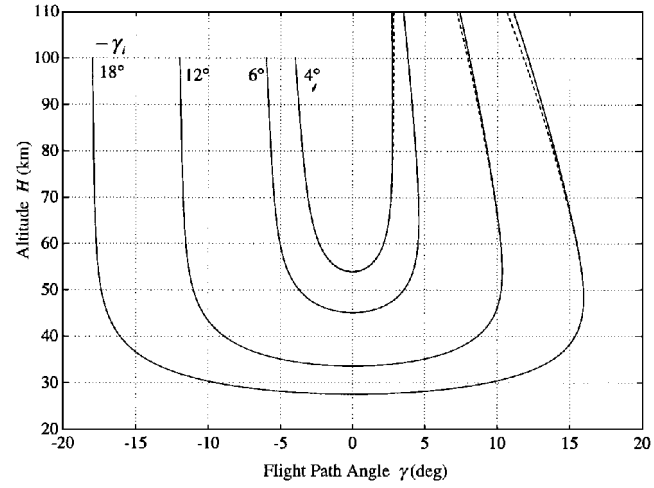

Fig. 3 Variation of flight-path angle as a function of altitude for various entry angles in three-dimensional skip trajectory.

of integration, is omitted for reasons of simplicity. In the solution of Eq. (35), we have defined the following functions:

$$F_1(\bar{\gamma}_0) \equiv \int [\ell n(1+\sin\bar{\gamma}_0) - \ell n(\cos\bar{\gamma}_0)]\,\mathrm{d}\bar{\gamma}_0$$

$$= -\cos\bar{\gamma}_0 + \frac{1}{9}\left(-3\cos\bar{\gamma}_0 + \cos^3\bar{\gamma}_0\right) + \cdots$$

$$F_2(\bar{\gamma}_0) \equiv \int \frac{\ell n(1+\sin\bar{\gamma}_0) - \ell n(\cos\bar{\gamma}_0)}{\cos\bar{\gamma}_0 - \bar{C}_2}\,\mathrm{d}\bar{\gamma}_0$$

$$= -\ell n(\cos\bar{\gamma}_0 - \bar{C}_2) - \frac{1}{3}\left[-\frac{1}{2}\cos^2\bar{\gamma}_0 - \bar{C}_2\cos\bar{\gamma}_0 + \mu\,\ell n(\cos\bar{\gamma}_0 - \bar{C}_2)\right] + \cdots \tag{36}$$

$$F_3(\bar{\gamma}_0) \equiv \int \frac{1}{\cos\bar{\gamma}_0 - \bar{C}_2}\,\mathrm{d}\bar{\gamma}_0$$

$$= \frac{-1}{\sqrt{\mu}}\left[\ell n\left(\frac{\mp\sqrt{\mu}\sin\bar{\gamma}_0 - \bar{C}_2\cos\bar{\gamma}_0 + 1}{\cos\bar{\gamma}_0 - \bar{C}_2}\right) + \ell n 2\right]$$

and

$$\mu \equiv 1 - \bar{C}_2^2 \tag{37}$$

where we take the minus sign for the descending arc and the plus sign for the ascending arc in function equation (36). Because the outer solutions for the perturbations f and p are zero, the composite solutions for f and p are identical to the inner solution of Eq. (35). Then, combining the fourth and fifth of the outer solution of Eq. (11) with inner solution of Eq. (35), the second-order solutions for ϕ and θ are of the form

$$\phi^c = \phi_c + f_c = \phi_0 + \varepsilon\bar{f}_0$$
$$\theta^c = \theta_c + p_c = \theta_0 + \varepsilon\bar{p}_0 \tag{38}$$

The structure of the solutions is elegant in the sense that it reveals the physical phenomenon in terms of mathematic description. The first term in Eq. (28) represents the Keplerian motion without atmospheric influence. On the other hand, the second term represents small perturbations due to the effect of aerodynamic force in the inner region.

Numerical Applications

The purpose of this section is to discuss the relative merits and the ranges of application for the analytic solutions obtained by using the iMAE. As numerical examples, we consider the three-dimensional motion of a space vehicle entering the Earth's atmosphere. The

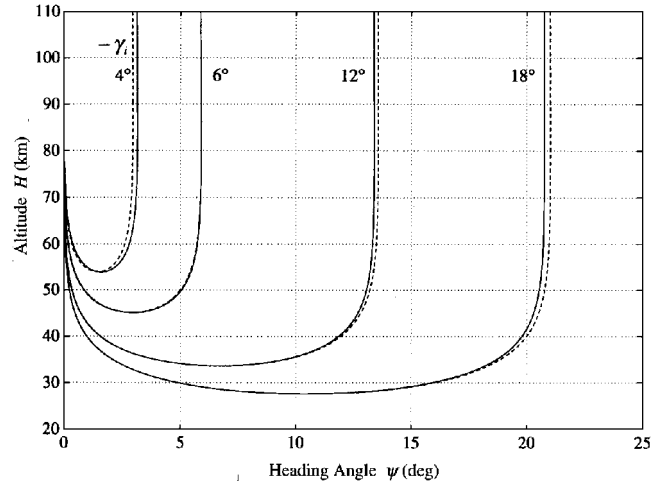

Fig. 4 Variation of heading angle as a function of altitude for various entry angles in three-dimensional skip trajectory.

vehicle has a maximum lift-to-drag ratio of $E^* = 1$ with physical parameter $B = 2.68$, starting with the initial entry speed $V_i = 1.1V_c$, i.e., $u_i = 1.21$ and using $\lambda = 1$, $\sigma = 30$ deg. Without loss of generality, we set other variables at the initial entry altitude $h_i = 0.0157$ to be zero, that is, $[\psi_i, \phi_i, \theta_i] = [0, 0, 0]$. Figures 2 and 3 plot the speed ratio $V/\sqrt{(g_s r_s)}$ and the flight-path angle γ as functions of the altitude. Dashed lines indicate the numerical solutions, and solid lines represent the iMAE solutions. The accuracy of the solutions is excellent because, as shown in Table 1, we have obtained six significant digits at the lowest point. Table 1 presents the numerical results of the trajectory variables at the bottom and at exit. In each set of data, the upper value is the pure numerical solution and the lower value is computed by our iMAE solutions. From Table 1, we see that the relative error for the speed is about 0.2% at the bottom and it propagates to 0.7% at exit for the worst case of $-\gamma_i = 4$ deg. Because the iMAE solutions are very accurate throughout the descending phase, the solutions are competent for evaluation of the critical elements at the peak deceleration and the maximum heating, which always occur before the lowest point is reached. However, because of the basic condition of the MAE technique, the solutions are less accurate for entry at small angles when the various forces involved are of the same order of magnitude throughout the trajectory. We suggest a completely different approach to analyze the case of entry with small angles.[9] Figures 4–6 present variations of the heading angle, latitude, and longitude as functions of altitude. For the initial entry angle $-\gamma_i = 4$ deg, there is some discrepancy between the numerical solution and the iMAE solution, as shown in Fig. 5. Even though the relative error for this case is large, the difference is only 0.069 deg in absolute value for the latitude at

Table 1 Comparison of trajectory elements ($\sqrt{u}, \gamma$) at bottom and at exit for various entry angles

Trajectory elements		Flight-path angle $-\gamma_i$, deg			
		4	6	8	12
Bottom altitude h_b	Numerical	0.0084587	0.0070730	0.0062788	0.0052702
	iMAE	0.0084470	0.0070704	0.0062783	0.0052708
Bottom speed $u_b^{1/2}$	Numerical	1.0516406	1.0009038	0.9570115	0.8788922
	iMAE	1.0466288	0.9989403	0.9562586	0.8791299
Exit speed $u_e^{1/2}$	Numerical	0.9901114	0.8918307	0.8117041	0.6781483
	iMAE	0.9828935	0.8914917	0.8137913	0.6819361
Exit angle $-\gamma_e$, deg	Numerical	2.8186071	3.8039602	5.1206997	7.9369104
	iMAE	2.7141180	3.8122696	5.1839038	8.0714158

Table 2 Comparison of trajectory elements (ψ, ϕ, θ) at exit for various initial entry angles

Trajectory elements		Flight-path angle $-\gamma_i$, deg			
		4	6	8	12
Heading angle ψ_e, deg	Numerical	2.9344642	5.8764035	8.5237840	13.559225
	iMAE	3.1321319	5.8789130	8.4401482	13.382860
Latitude ϕ_e, deg	Numerical	0.5140644	0.7370882	0.8241616	0.9069345
	iMAE	0.5829793	0.7557625	0.8289606	0.9037549
Longitude θ_e, deg	Numerical	18.603317	13.167788	10.178101	7.0592236
	iMAE	19.332678	13.354608	10.307469	7.2076078

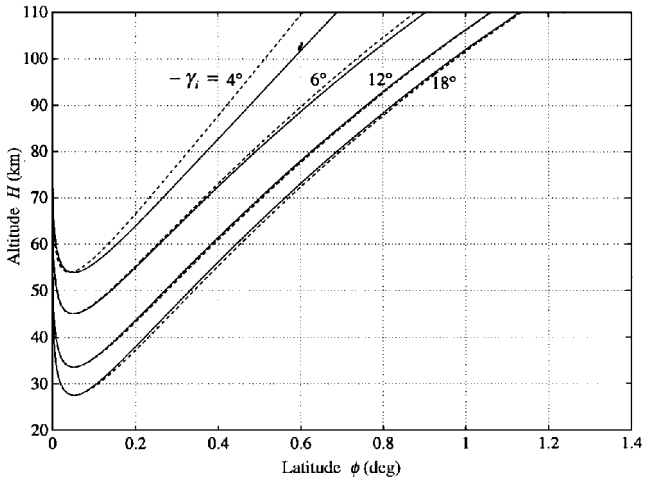

Fig. 5 Variation of latitude as a function of altitude for various entry angles in three-dimensional skip trajectory.

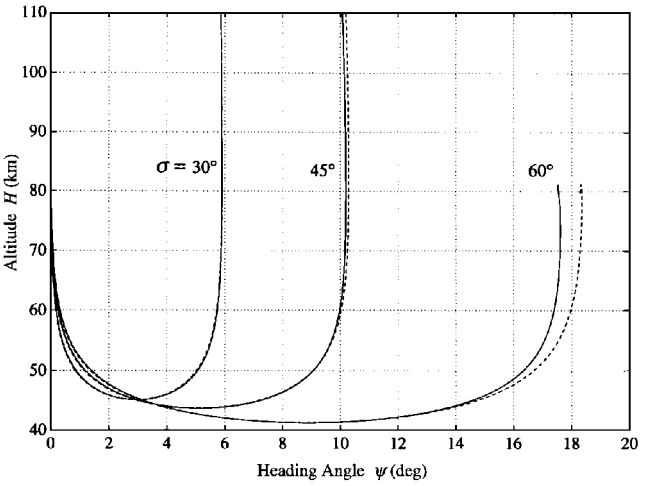

Fig. 7 Variation of heading angle as a function of altitude for various bank angles in three-dimensional skip trajectory.

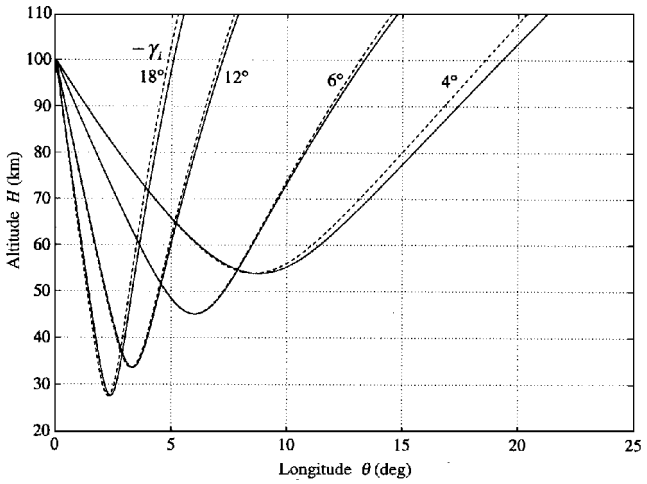

Fig. 6 Variation of longitude as a function of altitude for various entry angles in three-dimensional skip trajectory.

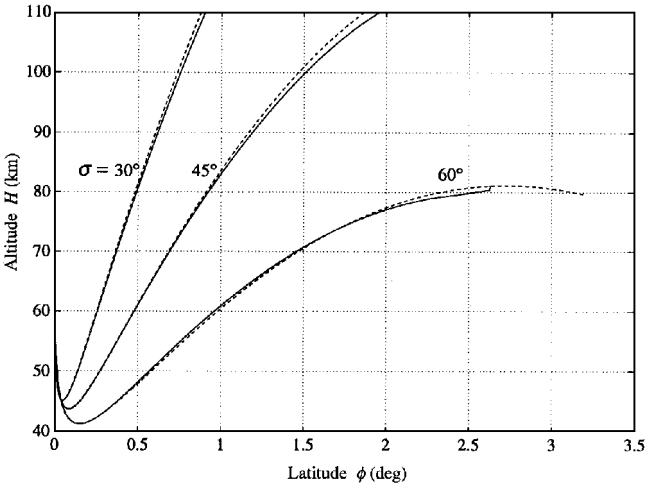

Fig. 8 Variation of latitude as a function of altitude for various bank angles in three-dimensional skip trajectory.

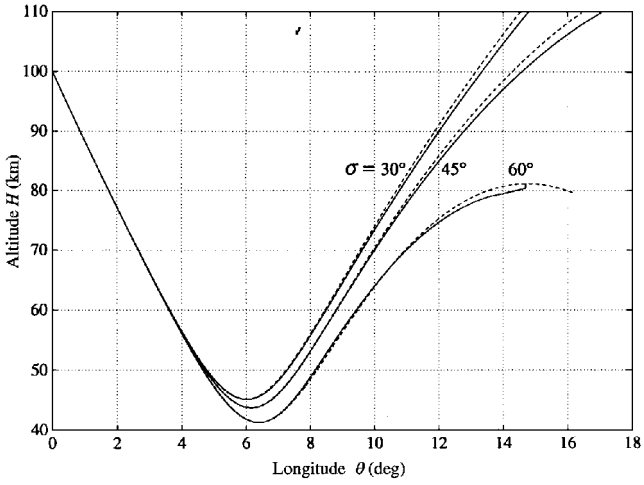

Fig. 9 Variation of longitude as a function of altitude for various bank angles in three-dimensional skip trajectory.

exit. Table 2 compares numerical results at exit for various entry angles.

To study the effect of the bank angle on the three-dimensional skip trajectory, we consider atmospheric entry with the same initial speed and altitude at the initial entry angle $-\gamma_i = 6$ deg for three values of bank angles, $\sigma = 30, 45$, and 60 deg. The variations of the trajectory variables as functions of the altitude for these cases are plotted in Figs. 7–9. Again, dashed lines represent the numerical solutions and solid lines represent the iMAE solutions. The space vehicle fails to skip out with the bank angle at 60 deg, and the relative error becomes larger when the bank angle is larger. Nevertheless, in Figs. 8 and 9, the iMAE solutions for latitude and longitude remain in good agreement with the numerical solutions for the three bank angles.

Conclusions

In this paper, an iMAE is proposed for deriving the second-order solutions of nonlinear differential equations that govern dynamic systems with controlling forces varying widely between the endpoints. The improved solutions obtained by the proposed technique are expressed in two parts: the first-order composite solutions and the composite solutions of the perturbations, which are the differences between the first-order composite solutions and the exact solutions. The first-order composite solutions and the composite solutions of the perturbations consist of outer solutions, inner solutions, and the common limits of the outer and inner solutions. To investigate the applicability and efficiency of the proposed technique, we applied it to analyze the three-dimensional atmospheric re-entry problem. In the process, for the matching we extended the endpoint in the outer region to validate the assumptions of outer expansions with one dominant force, and we created the boundary condition for the inner limit to strictly enforce the strong aerodynamic force assumption of inner expansions.

The improved matched asymptotic solutions are very accurate when compared with the pure numerical solution of the equations of motion. For skip trajectory with an error in the sixth or seventh digit for the altitude, it is not necessary to go to further higher-order terms to improve on the final solutions. Along with the solutions for speed and flight-path angle, the analytic solutions for heading change, latitude, and longitude were obtained and tested in a wide range of entry conditions. The accuracy of the analytic solutions was satisfactorily assessed and evaluated at the lowest altitude and at exit. The numerical results from the analytic solutions show excellent agreement with the pure numerical solutions. Because the solutions are in explicit form and are uniformly valid in both the Keplerian and the atmospheric regions, the trajectory elements at exit can be expressed explicitly.

In conclusion, an iMAE has been developed to analyze the three-dimensional motion of the atmospheric skip trajectory. The second-order solutions obtained by the improved method apply to all phases of flight from the vacuum through the atmosphere to either skip out or effective entry with a high degree of accuracy. The numerical results clearly demonstrate the applicability and flexibility of the improved technique.

References

[1] Prandtl, L., "Motion of Fluids with Very Little Viscosity," NACA Translation 452, 1928.

[2] Bretherton, F. P., "Slow Viscous Motion Round a Cylinder in a Simple Shear," *Journal of Fluid Mechanics*, Vol. 12, April 1962, pp. 591–613.

[3] Lagerstrom, P. A., and Kevorkian, J., "Earth-to-Moon Trajectories in the Restricted Three-Body Problem," *Journal Mécanique*, Vol. 2, No. 2, 1963, pp. 189–218.

[4] Breakwell, J. V., and Perko, L. M., "Matched Asymptotic Expansions, Patched Conics, and the Computation of Interplanetary Trajectories," *Progress in Astronautics and Aeronautics*, edited by R. L. Duncombe and V. G. Szebehely, Vol. 17, Academic, New York, 1966, pp. 159–182.

[5] Shi, Y. Y., Pottsepp, L., and Eckstein, M. C., "A Matched Asymptotic Solution for Skipping Entry into Planetary Atmosphere," *AIAA Journal*, Vol. 9, No. 4, 1971, pp. 736–738.

[6] Shi, Y. Y., "Matched Asymptotic Solution for Optimum Lift Controlled Atmospheric Entry," *AIAA Journal*, Vol. 9, No. 11, 1971, pp. 2229–2238.

[7] Busemann, A., Vinh, N. X., and Culp, R. D., "Solution of the Exact Equations for Three-Dimensional Atmospheric Entry Using Directly Matched Asymptotic Expansions," NASA Rept. CR-2643, March 1976.

[8] Vinh, N. X., and Kuo, Z.-S., "Improved Matched Asymptotic Solutions for Deceleration Control During Atmospheric Entry," Forty-Fifth Congress of the IAF, IAF Paper 94-A.2.012, Jerusalem, Israel, Oct. 1994.

[9] Longuski, J. M., and Vinh, N. X., "Analytic Theory of Orbit Contraction and Ballistic Entry into Planetary Atmospheres," Jet Propulsion Lab., Publication 80-58, California Inst. of Technology, Pasadena, CA, Sept. 1980.

J. A. Martin
Associate Editor